Journal of Building Engineering 80 (2023) 107656

Contents lists available at ScienceDirect

Journal of Building Engineering

journal homepage: www.elsevier.com/locate/jobe

Improving aerodynamic response of tall buildings using smart morphing facades

Smrithi Preetha Hareendran [a], Alice Alipour [a,*], Partha Sarkar [b]

[a] Department of Civil, Construction and Environmental Engineering, Iowa State University, Ames, IA, USA
[b] Department of Aerospace Engineering, Iowa State University, Ames, IA, USA

A B S T R A C T

Slender buildings are prone to vortex-induced vibrations and turbulence-induced buffeting. Usually, vortex-induced vibrations govern the strength and serviceability design criteria. The building's shape determines the aerodynamics of it; therefore, optimizing building shape can greatly reduce wind-induced vibrations. With a growing industry in adaptive and double-skin facades—mainly for energy saving purposes—there is an opportunity to innovate and implement smart, morphing facade modules (which we refer as *Smorphacades*) that actively modify their aerodynamic shape to alleviate flow-induced vibrations during high winds. This paper evaluates the performance of a 44-story tall building with the different configurations of the developed *Smorphacade* module system in mitigating building vibrations. Dynamic nonlinear time history analysis of the building under varying wind speeds ranging between 35 and 75 m/s are performed to evaluate the performance of building equipped with *Smorphacade* at low and high wind speeds. The performance measures chosen in the study are displacements and accelerations. Structural responses of building equipped with *Smorphacade* are compared against the bare building model responses to evaluate improvements in performance. Acceleration response comparisons at lower wind speeds provide insights into *Smorphacade* contributions to improving occupant comfort. Displacement comparisons at high wind speeds help understand the improvements in overall structural performance by reducing nonlinear response.

1. Introduction

In recent years, wind hazards, due to hurricanes, thunderstorms, gust fronts, tornadoes, and microbursts, have caused enormous safety concerns and economic losses, imposing extra burdens on building owners. The iconic building in Lake Charles, Louisiana, which is still empty months after Hurricane Laura (Pasch et al., 2020 [1]) is a glaring example of not only immediate but also long-term consequences of building vulnerability to extreme wind events. This situation is often exacerbated in buildings located in urban regions, where the surrounding clusters of tall buildings add to the magnitude and complexity of wind load effects. An example of this phenomenon was observed in Hurricane Ike where the urban aerodynamics led to a wind event not anticipated in the original design, leaving extensive damage to building envelopes (FEMA P-757 [2]). Such damages are, however, not isolated to extreme events. A recent lawsuit filed by the owners of 432 Park Avenue which is the tallest residential building in New York City, reports serviceability issues due to 'intolerable' noise. In another recent case, the Chinese SEG Skyscraper started wobbling and swaying in very mild winds, scaring the occupants, which led to the immediate evacuation of the building. Despite advances made in wind engineering, the range of damage and the extent of functionality loss witnessed by the building sector underline the importance of moving toward a new generation of smart buildings that can form the backbone of smart and resilient communities.

The aerodynamics of tall buildings can have a major impact on their design. The main structural system is a large part of the cost, and for tall buildings, wind is the governing lateral load. Keeping the motions of the tall building within comfortable limits is often a larger challenge than meeting structural strength requirements (Irwin, 2009 [3]; Xie, 2014 [4]). A common approach to alleviating

* Corresponding author.
E-mail address: alipour@iastate.edu (A. Alipour).

https://doi.org/10.1016/j.jobe.2023.107656
Received 6 March 2023; Received in revised form 19 July 2023; Accepted 23 August 2023
Available online 13 September 2023

wind vibrations on a building is to use structural control, which involves modifying the stiffness, mass, or damping of the building. Changing the mass and stiffness of a structure is costly and inefficient. Different passive dampers have been proposed, such as tuned mass dampers (Aly, 2012 [5]; Giaralis & Petrini, 2017 [6,7]; Kang et al., 2011 [8]; Kareem et al., 1999 [9]; Liu et al., 2008 [10]; Rana & Soong, 1998 [11]), tuned liquid dampers (Bauer, 1984 [12]; Shum & Xu, 2004 [13]; Xu et al., 1992 [14]), viscous dampers (Ankireddi & Yang, 2000 [15]; Chen & Bao, 2012 [16]; McNamara & Taylor, 2003 [17]; Nicos Makris et al., 1993 [18]), belt trusses and outriggers (Asai et al., 2013 [19]; Ho, 2016 [20]; Malekinejad & Rahgozar, 2011 [21]; Nanduri et al., 2013 [22]; Po Seng Kian, 2001 [23]; Rahgozar & Sharifi, 2009 [24]), and, recently, friction dampers (Cao et al., 2015, 2016 [25,26]). However, all of these control mechanisms have restricted applicability due to their limited maximum capacity, limited ability to tune to different frequencies and intensities, and a large space requirement for installation (multiple stories normally at higher levels of the building where the real estate value is higher). Numerous studies have discussed the application of passive and semi-active control strategies for mitigating structural vibrations under wind, but very few have transitioned to field applications for wind mitigation purposes. This is because control systems typically have limited performance bandwidth, and they are constrained to providing design performance for only the first mode of vibration (Yang. et al., 2000 [27]). Furthermore, problems arise with tuning of the designed dampers.

Both wind turbulence and vortex shedding tend to produce vibrations in tall buildings, whereas aerodynamic instabilities such as damping-driven flutter, although extremely rare, is possible at high wind speeds in a tall building if it is very slender and bluff shaped. Vortex excitations specifically result in oscillatory across-wind forces at a frequency, N_s, which is linearly proportional to the mean wind speed through the Strouhal number, St (a function of the shape of the bluff body). When N_s matches the frequency N_r of the building for a small range of wind speeds, resonance results in an amplified across-wind response. Measures such as stiffening and adding mass (increasing weight and cost) or introducing supplementary damping systems are mitigation measures that do not reduce the source of vortex shedding due to building shape. However, it is possible to alleviate vortex shedding forces through modification of the building shape. Passive approaches such as softened corners (Amin & Ahuja, 2010 [28]; Huang et al., 2015 [29]; Okamoto & Uemura, 1991 [30]), tapering and setbacks (Y. C. Kim & Kanda, 2013 [31]; Y. Kim & Kanda, 2010 [32]), varying cross section, spoilers (Chan et al., 2010 [33]; Ilgin & Gunel, 2007 [34]), and adding porosity or openings (Bitog et al., 2011 [35]; You & Kim, 2009 [36]) have been tested, and while they can be relatively effective, they do not address vibration issues from wind directionality.

Numerous studies have been conducted on double skin facades (DSF) for shape optimizations, porosity, and gap width between the façade skins since early 2000s to mitigate wind loads on tall buildings. Da Silva and Gomez (2008) [37] explored the effects of structural properties DSF on wind pressure distributions and Moon (2009) [38], Azad et al. (2013) [39], Samali et al. (2014) [40], Hu et al. (2017a, 2017b [41,42]), Giacheti et al. (2017, 2019 [43,44]) and Pomaranzi et al. (2020) [45] studied the structural capabilities of DSF systems on tall building motion control using shape optimizations and use of permeable outer skin layer. However, all those configurations are optimized to obtain highest performance in a few critical wind loading cases and cannot adapt to variations in wind actions.

As an advancement to the rather fresh state-of-the-art use of facades to reduce wind effects on buildings, this study evaluates the performance of a novel smart, morphing façade module system in reducing the wind load effects on buildings, thereby reducing structural vibrations. The *Smorphacade* concept can dynamically modify the aerodynamic shape of the building surface in real time (Hou et al., 2023 [46]) considering the variations in wind speed and wind directions to limit wind-induced vibrations. For the initial design of *Smorphacade*, Hou et al. (2023) [46] developed a preliminary design of the façade arrangement that is used as the basis of the analytical performance assessment in this paper. In this study, the evaluation of efficiency of a *Smorphacade* is performed for multiple façade configurations with varying inclination angles of fins and porosities, set in a passive mode. It should be noted that the smart mode is not activated here and will be the subject of future studies highlighting the control features of the *Smorphacade*. Recognizing the importance of understanding the post-elastic response of structures under wind loads, the building equipped with different configurations of the *Smorphacade* will be exposed to extreme wind conditions that may result in nonstructural damage and/or some nonlinearity in response. The analytical model of the building is set in such a way that can capture these nonlinearities through a post-elastic response characterization. The example tall building used in the analysis here is a 44-story tall building, with a rectangular cross section of an aspect ratio, $B/D = 1.5$ with length $B = 45.7$ m, width $D = 30.5$ m, and height, $H = 160$ m. The building is subjected to buffeting wind loads over a range of wind speeds between 35 m/s and 75 m/s in the along- and across-wind, and torsional directions for a duration of 30 min. The aerodynamic coefficients such as drag, lift, moment coefficients for the various *Smorphacade* configurations are obtained from section model tests conducted in the AABL Wind and Gust Tunnel located in the Wind Simulation and Testing (WiST) Laboratory at Iowa State University.

This paper is organized as follows: review of the evolution of façade system technologies in building design, description of *Smorphacade* and details of the wind tunnel experiments to derive aerodynamic coefficients, description of PBWD and engineering damage parameters used in the study, description of the wind load model used in the study, case study with nonlinear dynamic time history analysis on the benchmark tall building and finally the results and discussions of the case study with evaluations on the performance of *Smorphacade*.

2. Façade systems for response reduction

A number of studies have explored the potential of optimizing façade designs to reduce building vibrations. Gerhardt and Janser (1994) [47] conducted experimental studies on the wind loading of porous façade systems. The experimental parameters chosen were building dimensions, porosity and gap width for open country exposure flow of wind speeds. The studies showed a decrease in net pressure with increasing the gap width and increasing building aspect ratio. Maruta et al. (1998) [48] studied the effects of increased surface roughness through addition of balconies on the wind pressures acting on building skin. The experimental studies were carried

out in wind tunnels with buildings at a scale of 1/300 under an urban terrain exposure and different types of balconies with varying surface roughness. The experimental data proved the influence of surface roughness on wind pressures which was studied with emphasis near the leading edge of the side wall.

Da silva and Gomez (2008) [37] studied pressure distributions on the inner face of a multi-story DSF building model using wind tunnel tests. Multiple DSF layouts with varying gaps were tested for several angles of attack. The inner wall pressure distribution was observed to be significantly different for the building model with DSF compared to the model without DSF. Multiple wind tunnel tests with a boundary layer velocity profile were performed over the DSF building model to obtain inner facade pressure distributions. Moon (2009) [38] studied the structural capabilities of DSF systems on tall building motion control. Energy dissipating mechanisms were introduced in the cavities of the façade and the connectors between the façade and primary structure was made very flexible so that the majority of vibrations were taken by the facades while limiting the structural vibration of the building itself. The study proposed increasing the damping ratio of connectors to limit the excessive movements in the facade.

Lou et al. (2012) [49] studied the pressure distributions on the exterior and interior walls of corridor double skin facades or DSF (no vertical cross movements) with horizontal separations at every floor level. Studies were conducted over different DSF layouts, spacings of gaps and several angles of attack on tall buildings. The pressure distributions were studied to evaluate the strength implications on the façade. It was found that both the gap inner pressure and net pressure on the external skin depend on the layout, air corridor width, and wind incidence. Montazeri et al. (2013) [50] focused on reducing the vibrations in balconies of high-rise buildings using a new façade system and also evaluated its effectiveness in improving occupant comfort. The system consisted of a staggered semi-open second-skin facade in front of the balconies, to shield them from wind. Hu et al. (2017, 2019) [41,42] studied the use of a double-skin façade system to control wind-induced vibration of buildings.

Giachetti et al. (2018, 2019) [43,44] explored the aerodynamic behavior of a building when a permeable layer was placed outside the primary building wall with narrow separation. Wind tunnel tests carried out under smooth flow at various angles of attack showed that even a very small magnitude of open-gap between the screen and the building influenced the fluid behavior significantly. The global aerodynamic coefficients were not significantly affected by the presence of the screen but a decrease in the slope of lift coefficients was observed indicating lower susceptibility to galloping. Pomaranzi et al. (2020) [45] examined the effects of porous double skin facades on the wind pressures on cladding and inner façade skin using wind tunnel tests. It was found that the inner façade pressure was reduced by more than 40% than the standard façade system.

Jafari and Alipour (2021a, 2021b) [51,52] studied the effects of façade shapes on the aerodynamic flow and pressure reduction on tall buildings. An optimized Smart façade shape was developed based on response surface methodology and genetic algorithm that reduced the wind-induced pressure on the building at all angles of attack (AOA). The new façade that changes configurations based on

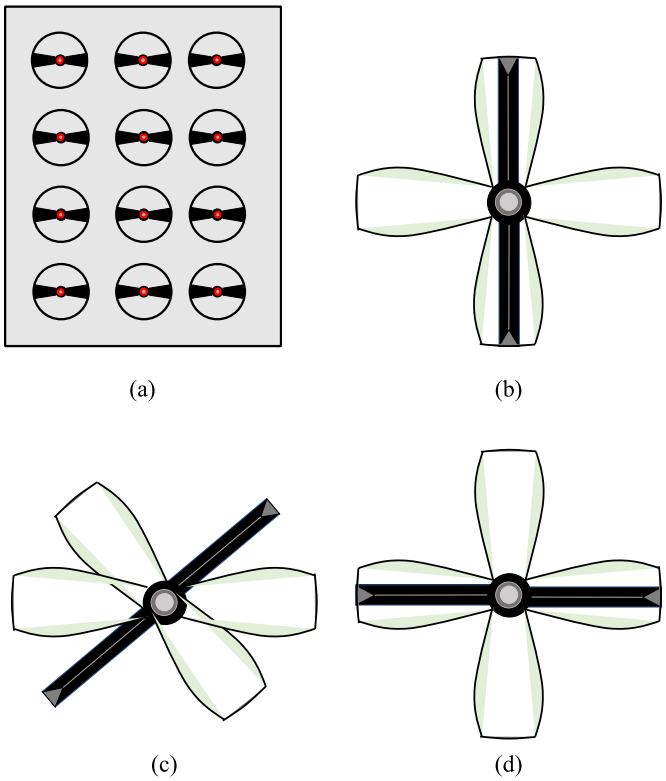

Fig. 1. (a) The stationary fan of the Smorphacade and the fan-fin assembly that rotates on top of the stationary fan in the Smorphacade for configurations (b) #1 (c) #2, and (d) #3.

AOA also reduced the vortex induced response by interrupting the flow separation. Among the shapes chosen for the study, a rectangular façade shape was identified as preferable due to simplicity in construction and aerodynamic performance.

From the studies mentioned here, it is evident that the presence of a secondary façade with varying porosity and roughness could help alleviating the effects of wind loads on buildings. However, all the studies mentioned here have geometrical restrictions that limit their efficiency in mitigating the highly transient wind loads. As a result, this study proposes a novel smart morphing façade module system that can dynamically modify the aerodynamic shape of the building facade considering the variations in wind speed and wind directions to limit wind-induced vibrations. The Smart morphing façade system (*Smorphacade*) is tested for deflection and acceleration control of tall buildings using nonlinear dynamic time history analysis.

2.1. Smart morphing façade (Smorphacade)

The idea of smart façade system (*Smorphacade*) originated at Iowa State University. As a first stage to prove the applicability of the concept, Hou et al. (2023) [46] conducted a series of experiments using aeroelastic and section models of the benchmark CAARC building with numerous passive configurations of the proposed *Smorphacade*. The study presented here explores the efficiency of *Smorphacade* using nonlinear finite element analysis on mathematical models. Hou et al. presents very detailed descriptions on the configurations of *Smorphacade* system and morphing mechanisms highlighted in this paper. Hence, the authors have cited Hou et al. [46] wherever required to describe such mechanisms. The double façade configurations and the mechanism of controlling porosities adjusting to incident wind flow used in this study are obtained from Hou et al. The *Smorphacade* is comprised of a set of circular ducts embedded in a flat plate and arranged in a matrix formation that is fixed on the original façade but with a gap between the two facades. Each circular-shaped duct is comprised of two parts; a fixed base with alternate open and closed surfaces shaped like a fan-blade and a rotating part similar in shape like the fixed one but placed inside the fixed one and capable of rotation by a protruding fin. By rotating the fin, the porosity of the duct and the fin inclination angle can be simultaneously changed, enabling flow control through the duct. An illustration of the model showing the *Smorphacade* with various configurations placed along the height of the CAARC building is shown in Fig. 1(a)-(d). The fin and fan arrangement of the façade system shown in the figure is configured to adjust its orientations to control the incident wind actions onto building surfaces. This is achieved by adjusting the porosity of the overall system as each unit is capable of independently adjusting orientations as dependent on the direction of wind. The fins also increase surface roughness which aids in dispersing the turbulent wind actions on building facades. The fin orientation of various configurations used in the tests are given in Fig. 1(b)–1(d) and Table 1. Configurations #6 and #8 are not shown in the figures as they are made as a combination of the three primary configurations by alternating them in different faces of the building. Configuration #6 is made by using #1 and #3 on alternate faces whereas configuration #8 is made by using #2 and #3 on alternate faces. Studies on section models used to identify force coefficients were conducted by Hou et al. The aerodynamic force and moment coefficients for various *Smorphacade* configurations as obtained from wind tunnel tests using section models are given Table 2.

3. Analytical model development for nonlinear time history analysis

The study uses a rectangular configuration tall building model with a plan aspect ratio of 1.5:1 and 160 m high. The 3-D view and plan of the bare building model is shown in Fig. 2(a) and (b). The model was designed as per the provisions of AISC-360 (2016) [53] to withstand structural loads imposed by ASCE-07 (2016) [54] specific to Miami-Dade county, FL. The detailed static design of the building using SAP2000 is given in Hareendran et al. (2022) [55]. The building model was later translated into an OpenSees model for the purpose of nonlinear time history analysis. The material and element libraries available in OpenSees was chosen for the frame elements in the model. Further information on OpenSees modeling is presented by the authors in Hareendran et al. (2023) [56]. Uniform area loads were used in the analytical model for dead and live loads. The turbulent wind loads were applied as nodal forces in the along- and across-wind directions. The modal frequencies corresponding to the first five modes for the buildings are given in Table 3. The modes of vibrations in the first two mode shapes of the building were longitudinal and lateral while the fifth mode corresponds to the first non-uni-planar (combination of flexural and torsional) mode.

Wind loads acting on tall buildings are non-uniform in nature and contain a range of frequencies. The fluctuating component of wind along the height of buildings leads to turbulence-induced and motion-induced loads acting over sustained durations. The wind-induced response of a tall building at any height and time can be expressed in terms of the buffeting (turbulence-induced) and self-

Table 1
Various configurations of Smorphacade used in the study.

Configuration No.	For all AOA	Face of the Building			
		# 1	# 2	# 3	# 4
1	Fin inclination	45°	45°	45°	45°
	Porosity (%)	54.7	54.7	54.7	54.7
2	Fin inclination	90°	90°	90°	90°
	Porosity (%)	76.4	76.4	76.4	76.4
3	Fin inclination	0°	0°	0°	0°
	Porosity (%)	54.7	54.7	54.7	54.7
6	Fin inclination	0°	45°	0°	45°
	Porosity (%)	54.7	54.7	54.7	54.7
8	Fin inclination	0°	90°	0°	90°
	Porosity (%)	54.7	76.4	54.7	76.4

Table 2
Aerodynamic coefficients and their derivatives of the façade configurations.

Mean Aerodynamic Force Coefficients									
Config. No.	Angle of Attack = 0°			Angle of Attack = 34°			Angle of Attack = 90°		
	C_D	C_L	C_M	C_D	C_L	C_M	C_D	C_L	C_M
0	1.10	−0.06	−0.02	1.44	0.42	0.03	1.73	−0.01	−0.02
1	1.03	−0.06	−0.02	1.38	0.29	0.05	1.47	−0.13	−0.02
2	0.98	−0.22	−0.05	1.37	0.28	0.05	1.49	−0.17	−0.02
3	1.08	−0.09	−0.02	1.46	0.35	0.05	1.55	−0.07	−0.02
6	1.06	−0.09	−0.02	1.42	0.27	0.04	1.49	−0.13	−0.02
8	1.03	−0.12	−0.03	1.38	0.21	0.04	1.44	−0.11	−0.02
Derivatives of Mean Aerodynamic Force Coefficients									
Config No.	Angle of Attack = 0°			Angle of Attack = 34°			Angle of Attack = 90°		
	$dC_D/d\theta$	$dC_L/d\theta$	$dC_M/d\theta$	$dC_D/d\theta$	$dC_L/d\theta$	$dC_M/d\theta$	$dC_D/d\theta$	$dC_L/d\theta$	$dC_M/d\theta$
0	0.00	−4.65	−0.35	0.69	0.24	0.19	0.00	−2.33	−0.29
1	0.00	−4.90	−0.66	0.94	0.51	0.22	0.00	−2.75	−0.29
2	0.00	−4.91	−0.82	0.65	0.59	0.23	0.00	−3.22	−0.31
3	0.00	−4.74	−0.53	0.82	0.29	0.19	0.00	−2.50	−0.295
6	0.00	−5.10	−0.65	0.86	0.35	0.20	0.00	−2.44	−0.27
8	0.00	−4.92	−0.72	0.67	0.31	0.21	0.00	−2.71	−0.31

Configuration #0 represents the bare building model.

excited (motion-induced) loads. The self-excited loads have gained importance in wind response studies involving long-span bridges, but are usually neglected in case of buffeting analysis of tall buildings. However, as the tall buildings continue to grow slender, consideration of self-excited loads in buffeting analysis becomes more critical. Hence, the effects of such loads is incorporated into the damping formulations for the building used in this study. The mathematical formulations of these loads used in the study is adopted from Hareendran et al. (2022) [55]. The aerodynamic load coefficients used in the calculation of buffeting and self-excited loads were extracted from wind tunnel studies (Hou and Sarkar, 2023 [46], Hareendran et al., 2022 and 2023 [55,57]).

The effectiveness of various façade configurations was tested by subjecting the building model to long durations (30 min) of wind loads corresponding to different magnitudes of 3-sec gust speeds varying between 35 m/s to 75 m/s at 10 m elevation. The aerodynamic load coefficients and their derivatives with respect to angle of attack (0°, 34° and 90°) as used in the wind load calculations for various *Smorphacade* configurations are given in Table 2. The mean wind speed variation along the height of the building was calculated using the power law equation corresponding to a suburban terrain (power-law exponent). The wind speed variation based on power law is shown in Fig. 2(a). The fluctuating velocity components of the wind time histories were generated for each floor level of the building considering the spatial coherence functions between the velocity fluctuations at different heights along the building. The wind load time histories that are generated by considering different tributary areas in the external and internal panels are applied at the nodes at every floor level of the building.

4. Results and discussion

Based on the time history analysis, structural displacements and accelerations of the building were extracted to evaluate effectiveness of *Smorphacade* and compare performance of different configurations. Melbourne and Palmer (1992) [58] observed that root mean square (RMS) accelerations can be a good representation of the occupant comfort over a period of time rather than occasional peak accelerations. Hence, in this study peak displacements and RMS accelerations are chosen as the damage parameters to evaluate the performance of given *Smorphacade* configurations. The building section with the building's degrees-of-freedom or coordinate-axes and the three angles of attack of wind loads are shown in Fig. 2(f). Displacements and RMS accelerations in the along-wind and across-wind directions are obtained and compared for effectiveness. The effectiveness of each configuration is calculated in comparison to the bare building model, i.e. building with no façade. Hence effectiveness of each façade is given as:

$$E = \frac{Parameter_{Bare} - Parameter_{Facade}}{Parameter_{Bare}} \times 100 \quad (1)$$

where $Parameter_{Bare}$ is the RMS acceleration/displacement of the bare building model and $Parameter_{Facade}$ is the RMS acceleration/displacement of the building with the addition of *Smorphacade*. The comparison of structural responses with and without *Smorphacade* used in the study are shown in Fig. 3. The responses are shown for a 3-sec wind speed of 35 m/s at 10 m elevation and 0° AOA. Response ratios are with respect to bare building model that is used to represent the horizontal axes in the sub-figures. These sub-figures show significant structural response reduction with the addition of *Smorphacade* in all of the cases except Configuration #2 that shows enhancement of accelerations in along-wind direction. Expanding on the results, Fig. 4 is given to show the effectiveness of the different configurations in inhibiting structural motions under varying AOA. Fig. 4(a) and (b) show the acceleration reduction in terms of effectiveness percentage as described earlier in the along- and across-wind directions. Most effective and least effective configurations for each AOA is highlighted in the figures.

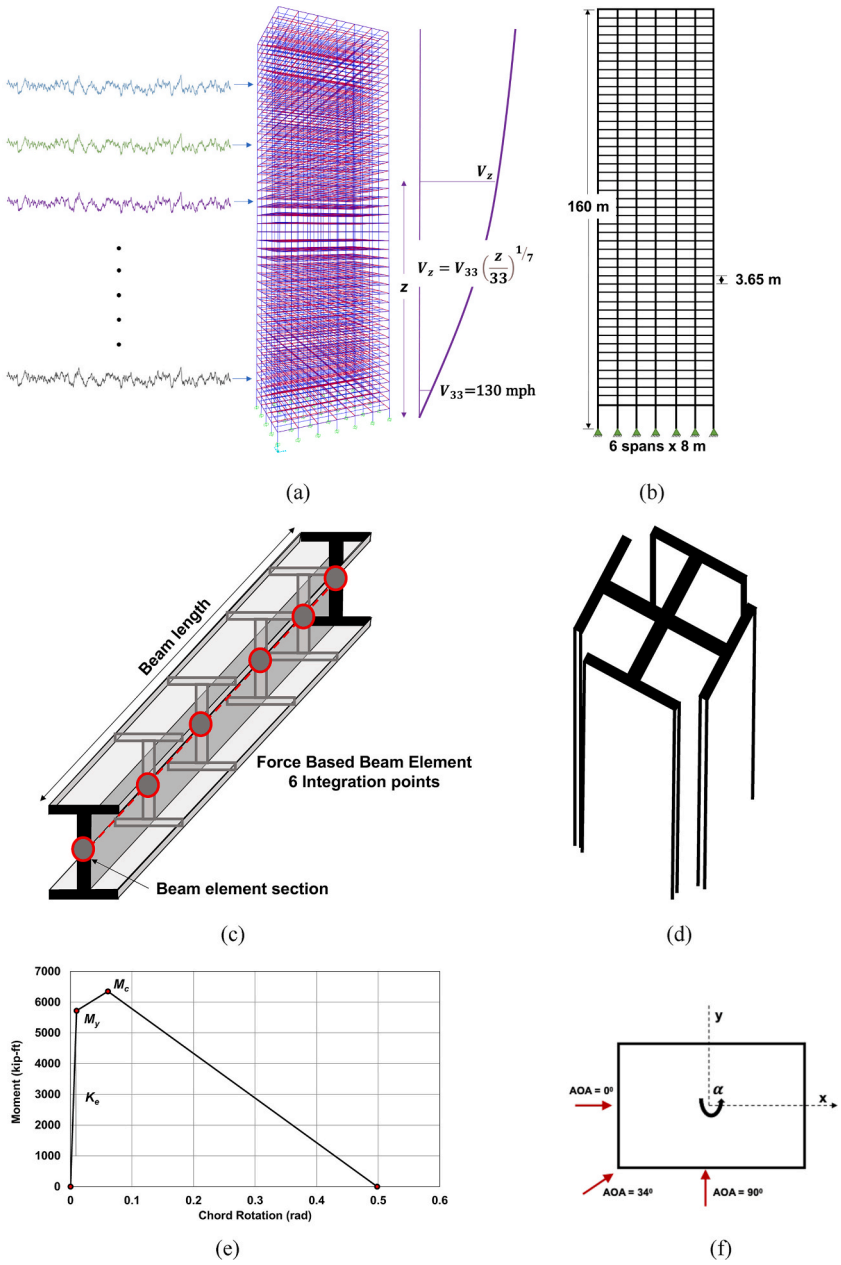

Fig. 2. (a) Isometric view of the 44-story building with the wind actions on the left and power law to calculate wind speeds along the height on the right, (b) basic geometric dimensions, (c) force-based beam element used in FEA with the cross-section of wide-flanged beams used in the model, (d) column cross-section used, (e) Moment-curvature relationship of the beams used in the longitudinal direction, and (f) cross section of the building with directions of wind loading used in the study.

Table 3
Column and beam cross-sections used in the design of the 44-story building.

44 story building			
Floor level	Column (in)	Beam Long direction	Beam Short direction
1–10	CR 50 × 3 × 40 × 3	W 18 × 119	W 24 × 370
11–22	CR 50 × 3 × 30 × 3	W 18 × 119	W 24 × 370
23–33	CR 50 × 2 × 30 × 2	W 18 × 119	W 24 × 250
34–44	CR 50 × 2 × 20 × 2	W 18 × 119	W 24 × 250

Note: Columns are custom designed with dimensions noted in inches. Beams are standard hot rolled sections adopted from AISC steel manual.

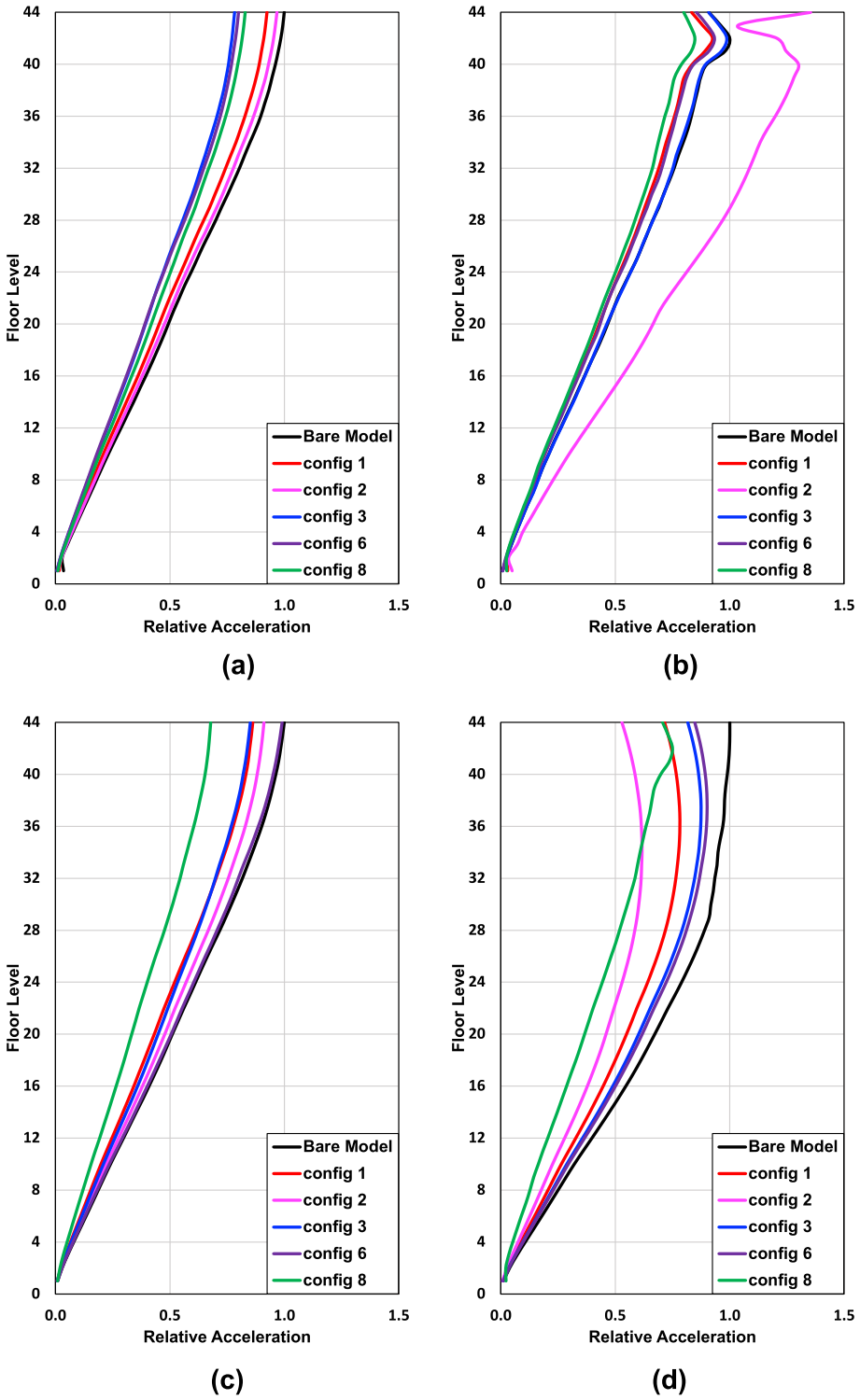

Fig. 3. Variation of peak structural responses for (a) across-wind acceleration, (b) along-wind acceleration, (c) across-wind displacement and (d) along-wind displacement along the height of building for various façade configurations at 35 m/s wind speed.

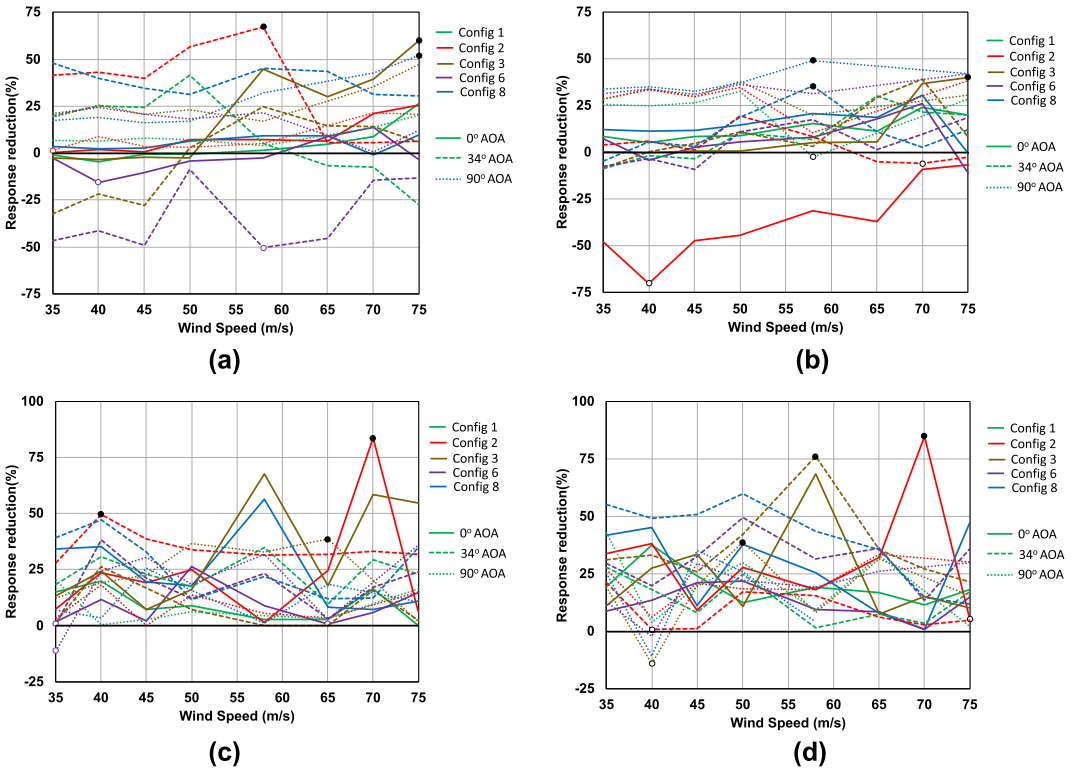

Fig. 4. Comparison of peak structural responses for (a) across-wind acceleration, (b) along-wind acceleration, (c) across-wind displacement and (d) along-wind displacement for different wind speeds (35–75 m/s) and varying AOA.

- Configuration #2 proves to be the most effective in resisting across wind accelerations for 34° AOA at the same time offering least resistance for along wind accelerations for the same AOA.
- Configuration #8 is observed to be highly efficient in mitigating accelerations in both directions for 34° and 90° AOA but does not perform so well for 0° AOA.

Fig. 4(c) and (d) show the comparisons of Smorphacade configurations in reducing peak displacements (top of the building) in the across-wind and along-wind directions, respectively. Fig. 4(c) shows all of the *Smorphacade* configurations being advantageous to the reduction of peak across-wind displacements, although the effectiveness varies widely.

- Configuration #3 can be seen to be most efficient in reducing peak across-wind displacements for 90° AOA at the same time being least efficient at 34° AOA for a wind speed of 65 m/s.
- Configuration #3 is the most effective in reducing peak along-wind displacements at design wind speed (58 m/s) for 34° AOA while being least efficient for a lower wind speed of 40 m/s and 90° AOA.

The wide variations in effectiveness of façade configurations for peak along-wind and across-wind responses with varying wind speeds shows the need for a dynamically varying capability. Façade systems such as *Smorphacade* is highly promising in the objective of building the most efficient structural systems. Table 4 shows the effectiveness of *Smorphacade* averaged over the entire range of wind speeds for all the AOAs. Based on the highlighted results, configurations #2, #3 and #8 proves to be the most effective.

- Configuration #2 is the most effective in reducing along-wind displacements for 0° and 90° AOA and configuration #8 is the most efficient for 34° AOA. Along-wind accelerations are reduced the most by configuration #8 for 0° and 90° AOA and configuration #3

Table 4
Results from the modal analysis of the building.

Mode Number	44 story building	
	Frequency (Hz)	Time Period (sec)
1	0.193	5.19
2	0.237	4.22
3	0.515	1.94
4	0.658	1.52
5	0.870	1.15

for 34° AOA. Upon, further examination configuration #8 is better for the overall along-wind response reduction for all AOA as configuration #2 has the worst performance in mitigating along-wind accelerations for 0° and 90° AOA.

- Configuration #3 is the most effective in reducing across-wind displacements for 0° and 90° AOA and configuration #2 is the most efficient for 34° AOA. Across-wind accelerations are reduced the most by configuration #3 for 0° AOA and configuration #8 for 34° and 90° AOA. Upon, further examination configuration #8 is better for the overall across-wind response reduction for all AOA when compared to configurations #2 and #3.

As seen in Fig. 4, the effectiveness of *Smorphacade* vary significantly with varying wind speeds as well. To further inspect this variation, the results are averaged over two ranges of wind speeds: winds up to design wind speed (<58 m/s) and winds greater than design wind speed (>58 m/s). These results are given in Table 5 (displacements) and 6 (accelerations). The results show increase in *Smorphacade* effectiveness for high wind speeds (>58 m/s) when compared to lower wind speeds. This could imply that *Smorphacade* is highly capable of limiting nonlinearity in structural responses at high wind speeds. Similar to previous observations configurations #2, #3 and #8 seem to be the most effective configurations overall. Configuration #6 is most efficient in reducing along-wind displacements and accelerations for 34° and 90° AOA, respectively (see Table 6).

Based on such inferences and observations here, it can be concluded that the effectiveness of *Smorphacade* is highly dependent on the fin inclination, porosity and wind speeds. The *Smorphacade* also exhibits high effectiveness for winds greater than the design wind speed. Thus, it can be concluded that with the provided versatility, *Smorphacade* can continuously change orientations to provide the highest efficiency and is capable of avoiding undesirable structural consequences.

5. Fragility curves and loss functions

Fragility analysis is used to calculate conditional probability of exceedance of displacements and accelerations to quantitatively assess damage states. The correlation between structural response and damage states are defined and detailed in the FEMA P-58 database. From the extensive database, three structural components are chosen in this study to illustrate the process. These are post-Northridge welded steel moment connections, bolted shear tab gravity connections and welded column splices given in Table 7 along with their damage state progression (see Table 8).

The fragility curves given in FEMA database for the given structural components are used to calculate losses. These fragility curves are used to interpolate the probability of exceedance for each damage state based on the chosen percentile of inter-story drift ratio and probability of exceedance of wind speed from the ASCE 07 hazard curve. The probability of exceedance corresponding to each damage state may be used to evaluate the losses due to repair or replacement of the component. The cost of repair/replacement for the fragility groups are also given by FEMA and can be obtained from the FEMA P-58 database. In this study, the loss ratio is the parameter used, which is the ratio of repair to replacement cost. So, if the loss ratio is reported as 1, it means the cost of repair is either equal to or greater than the cost of replacement and that the component must be replaced. The probability of exceedance corresponding to the highest percentile story drift ratio is obtained from the fragility curves. The study compares the losses computed for the bare building model and those equipped with *Smorphacade* for 0° AOA. The comparison of loss ratios for the fragility groups chosen in the study are given in Fig. 5. The predictions show similar results to those observed in Fig. 3 with the bare model having highest loss ratios for all damage states. *Smorphacade* configurations perform better resulting in lower losses over all wind speeds with the effectiveness increasing with increasing wind speeds.

6. Conclusions

Numerous studies have been completed over the past few decades to study the aerodynamic implications of using facades and shape optimization of such systems to limit tall-building motions. Only a few such studies have explored the geometrical modification of façade systems to obtain maximum reduction in surface pressures thereby reducing structural responses. However, all those

Table 5
Results showing the compared effectiveness of various façade configurations for peak structural responses averaged over the entire range of wind speeds.

AOA	Config	Along-wind displacement	Across-wind displacement	Average displacement reduction	Along-wind acceleration	Across-wind acceleration	Average acceleration reduction
0	1	19.9	9.2	14.6	12.8	4.4	8.6
	2	31.3	23.9	27.6	−36.7	8.8	−14.0
	3	23.1	32.5	27.8	11.2	20.5	15.9
	6	12.4	9.0	10.7	6.6	−2.1	2.3
	8	27.2	23.6	25.4	14.9	5.3	10.1
34	1	13.5	23.3	18.4	9.3	9.2	9.3
	2	8.7	34.8	21.8	3.2	33.2	18.2
	3	36.6	8.8	22.7	10.9	−2.5	4.2
	6	31.1	17.5	24.3	4.7	−33.8	−14.6
	8	40.2	26.5	33.4	10.6	37.9	24.3
90	1	20.1	7.6	13.9	22.5	9.4	16.0
	2	22.1	8.5	15.3	29.2	9.1	19.2
	3	17.0	23.4	20.2	30.1	26.9	28.5
	6	19.7	18.9	19.3	34.3	16.8	25.6
	8	17.0	11.7	14.4	38.3	28.0	33.2

Table 6
Results showing the compared effectiveness of various façade configurations for peak structural displacements averaged over lower wind speeds (<58 m/s) and higher wind speeds (>58 m/s).

AOA	Config	Wind speed <58 m/s			Wind speed >58 m/s		
		Along-wind displacement	Across-wind displacement	Average displacement reduction	Along-wind displacement	Across-wind displacement	Average displacement reduction
0	1	22.5	10.8	16.7	15.5	6.4	11.0
	2	25.5	15.3	20.4	40.9	38.1	39.5
	3	30.3	25.7	28.0	10.9	43.6	27.3
	6	15.1	10.1	12.6	8.0	7.1	7.6
	8	32.3	32.5	32.4	18.7	8.7	13.7
34	1	16.1	24.9	20.5	9.3	20.7	15.0
	2	11.2	36.4	23.8	4.6	32.2	18.4
	3	41.7	10.4	26.1	28.0	6.0	17.0
	6	32.6	19.2	25.9	28.5	14.8	21.7
	8	51.8	30.6	41.2	20.9	19.8	20.4
90	1	21.1	6.8	14.0	17.6	9.7	13.7
	2	18.1	8.2	13.2	31.9	9.3	20.6
	3	14.3	24.7	19.5	23.6	20.1	21.9
	6	16.4	18.7	17.6	27.9	19.3	23.6
	8	15.9	10.5	13.2	22.4	14.6	18.5

Table 7
Results showing the compared effectiveness of various façade configurations for peak structural accelerations averaged over lower wind speeds (<58 m/s) and higher wind speeds (>58 m/s).

AOA	Config	Wind speed <58 m/s			Wind speed >58 m/s		
		Along-wind acceleration	Across-wind acceleration	Average acceleration reduction	Along-wind acceleration	Across-wind acceleration	Average acceleration reduction
0	1	9.4	−1.0	4.2	18.4	13.4	15.9
	2	−48.2	3.4	−22.4	−17.7	17.6	−0.05
	3	1.4	6.8	4.1	27.5	43.2	35.4
	6	4.0	−7.2	−1.6	11.0	6.4	8.7
	8	14.0	4.8	9.4	16.3	6.1	11.2
34	1	0.6	23.1	11.9	23.9	−14.1	4.9
	2	7.9	49.8	28.9	−4.6	5.7	0.6
	3	2.2	−11.0	−4.4	25.5	11.5	18.5
	6	1.6	−39.4	−18.9	9.9	−24.4	−7.3
	8	11.7	39.6	25.7	8.7	35.0	21.9
90	1	21.3	6.4	13.9	28.7	9.4	19.1
	2	27.3	4.3	15.8	38.5	9.1	23.8
	3	30.0	21.1	25.6	30.4	26.9	28.7
	6	32.8	21.0	26.9	42.1	16.8	29.5
	8	37.6	20.3	29.0	42.0	28.0	35.0

Table 8
Structural components and damage progression adopted from FEMA P-58.

Structural Components	Damage Parameter	Damage States	Description	Median; Dispersion
Welded column splices	Story drift ratio	DS1/DS2 DS3	DS1: Ductile fracture of the groove weld flange splice. Damage in field is either obscured or deemed to not warrant repair. No repair conducted.	0.02; 0.4
			DS2: Ductile fracture of the groove weld flange splice	0.02; 0.4
			DS3: DS1 followed by complete failure of the web splice plate and dislocation of the two column segments on either side of the splice.	0.05; 0.4
Bolted shear tab gravity connections	Story drift ration	DS1/DS2 DS3,DS4	DS1: Yielding of shear tab and elongation of bolt holes, possible crack initiation around bolt holes or at shear tab weld. Damage in field is either obscured or deemed to not warrant repair.	0.04; 0.4
			DS2: Yielding of shear tab and elongation of bolt holes, possible crack initiation around bolt holes or at shear tab weld.	0.04; 0.4
			DS3: Partial tearing of shear tab and possibility of bolt shear failure (6-bolt or deeper connections).	0.08; 0.4
			DS4: Complete separation of shear tab, close to complete loss of vertical load resistance.	0.11; 0.4
Post-Northridge welded steel moment connection	Story drift ratio	DS1	DS1: Local beam flange and web buckling.	0.03; 0.3
		DS2	DS2: DS1 plus lateral-torsional distortion of beam in hinge region.	0.04; 0.3
		DS3	DS3: Low-cycle fatigue fracture in buckled region of reduced beam section.	0.05; 0.3

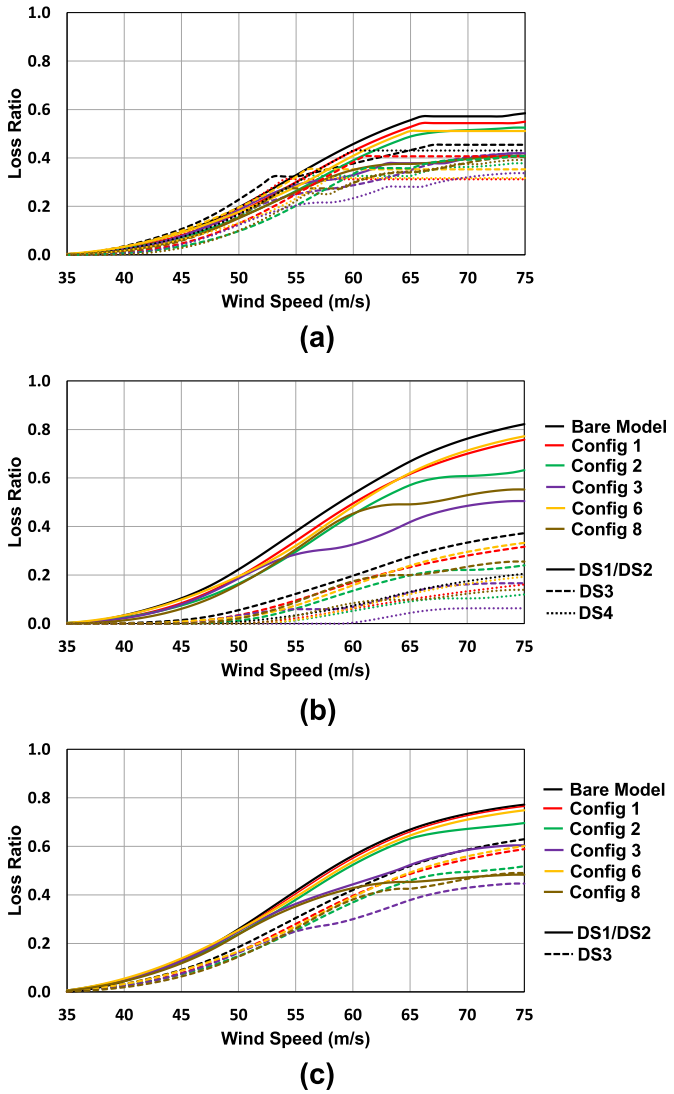

Fig. 5. Comparison of Loss Ratio curves for (a) Post-Northridge welded steel moment connections, (b) bolted shear tab gravity connections, and (c) Welded column splices for different wind speeds (35–75 m/s) and failure states for 0° AOA.

configurations were optimized to obtain highest performance in a few critical wind loading cases and were incapable of adapting to variations in wind actions. This study focuses on the numerical evaluation of performance of a novel smart, morphing façade module system (Smorphacade) developed at Iowa State University to mitigate the wind effects on buildings. Recognizing the importance of understanding the post-elastic response of structures under wind loads, this study considers the nonlinearity in response of buildings as well as the associated uncertainties in wind loading. *Smorphacade* is evaluated for its performance in the response control of tall buildings using nonlinear time history analysis. The tall building was subjected to buffeting wind loads over a range of wind speeds between 35 m/s and 75 m/s (3-sec gust at 10 m elevation) in the along-wind (along its length, B), across-wind (along its width, D), and diagonal directions corresponding to 0°, 90° and 34° angle of attack for a duration of 30 min. The aerodynamic drag, lift, moment coefficients and their derivatives for the various façade configurations were obtained from section model tests conducted in the AABL Wind and Gust Tunnel located in the Wind Simulation and Testing Laboratory (WiST) at Iowa State University by Hou et al. (2023).

Comparisons were drawn between different façade configurations for various angles of attack and the most efficient configuration was obtained based on the effectiveness in reducing accelerations and displacements in the across-wind and along-wind directions. The average effectiveness results show that the facades are highly efficient in limiting motions for all AOA. The discussions showed that different façade configurations are required for the overall building motion control and no one configuration can effectively control motions in all three degrees of motion simultaneously and for all wind directions considered here. This proves importance of a smart façade morphing capability of the proposed *Smorphacades*. The study shows the requirement and effectiveness of the proposed *Smorphacade* for building motion control. The effectiveness of *Smorphacade* for wind speeds over the design wind speed of the buildings also provides the advantage of limiting nonlinearity in structural behavior at high wind speeds thus minimizing structural damage and

losses.

Like any other mechanical system/façade added to the building, the *Smorphacade* are subjected to wear and tear and may require scheduled inspection and maintenance. The long-term performance of the *Smorphacade* requires a detailed life-cycle cost analysis that is out-of-scope of this paper. Similar studies have been completed by the authors in use of auxiliary dampers to the buildings for wind mitigation purposes (e.g., Micheli et al., 2020 [59–63]).

The current paper showed the positive impact of different activated modes of a *Smorphacade* for a rectangular building ($B/D = 1.5$). Further extensions of the work will include consideration of other shapes of buildings (different B/D rectangular) or other shapes of buildings to evaluate the feasibility of the developed *Smorphacade* on a larger stock of tall buildings.

Author statement

Conceptualization (Alice Alipour); Data curation (Smrithi Hareendaran): Formal analysis (Smrtihi Hareendran); Funding acquisition (Alice Alipour); Investigation (Smrithi Hareendran, Alice Alipour, Partha Sarkar); Methodology (Alice Alipour); Project administration (Alice Alipour); Resources (Alice Alipour); Supervision (Alice Alipour); Validation (Smrithi Hareendran); Visualization (Smrithi Hareendran); Roles/Writing - original draft (Smrithi Hareendran); Writing - review & editing (Alice Alipour and Partha Sarkar).

Declaration of competing interest

The authors declare that they have no known competing financial interests or personal relationships that could have appeared to influence the work reported in this paper.

Data availability

Data will be made available on request.

Acknolwedgements

This paper is based upon work supported by the National Science Foundation under Grants No. 2214039 and 1826356. This support is gratefully acknowledged. Any opinions, findings, and conclusions or recommendations expressed in this material are those of the authors and do not necessarily reflect the views of the sponsor.

References

[1] R.J. Pasch, R. Berg, D.P. Roberts, P.P. Papin, Hurricane Laura (AL 132020), Natl. Hurric. Cent. Trop. Cycl. rep. (2020).
[2] FEMA P-757, Hurricane Ike in Texas and Louisiana; Building Performance Observations, Recommendations and Technical Guidance, Federal Emergency Management Agency, Mitigation Assessment Team Report, 2009.
[3] P.A. Irwin, Wind Engineering challenges of the new generation of super-tall buildings, J. Wind Eng. Ind. Aerod. 97 (2009) 328–334.
[4] J. Xie, Aerodynamic optimization of super-tall buildings and its effectiveness assessment, J. Wind Eng. Ind. Aerod. 130 (2014) 88–98.
[5] A.M. Aly, Proposed Robust Tuned Mass Damper for Response Mitigation in Buildings Exposed to Multidirectional Wind, Struct. Des. Tall Spec. Build. (2012).
[6] A. Giaralis, F. Petrini, Wind-induced vibration mitigation in tall buildings using the tuned mass damper inerter, Procedia Eng. 199 (2017).
[7] A. Giaralis, F. Petrini, Optimum design of the tuned mass damper inerter for serviceability limit state performance in wind-excited tall buildings, J. Struct. Eng. 143 (2017).
[8] J. Kang, H.S. Kim, Mitigation of wind response of a tall building using semi-active tuned mass dampers, Struct. Des. Tall Special Build. 5 (2010).
[9] A. Kareem, T. Kijewski, Mitigation of Motions of Tall Buildings with Specific Examples of Recent Applications, Wind struct. vol. 2 (1999).
[10] M.Y. Liu, W.L. Chiang, J.H. Hwang, C.R. Chu, Wind induced vibration of high-rise building with tuned mass damper including soil-structure interaction, J. Wind Eng. Ind. Aerod. 96 (2008).
[11] R. Rana, T.T. Soong, Parametric study and simplified design of tuned mass dampers, Eng. Struct. 20 (1998).
[12] H.F. Bauer, Oscillations of immiscible liquids in a rectangular container: a new damper for excited structures, J. Sound Vib. 93 (1984).
[13] K.M. Shum, Y.L. Xu, Multiple tuned liquid column dampers for reducing coupled lateral and torsional vibration of structures, Eng. Struct. 26 (2004).
[14] Y.L. Xu, K.C.S. Kwok, B. Samali, The effect of tuned mass dampers and liquid dampers on cross-wind response of tall/slender structures, J. Wind Eng. Ind. Aerod. 40 (1992).
[15] S. Ankireddi, H.T.Y. Yang, Directional mass dampers for buildings under wind or seismic loads, J. Wind Eng. Ind. Aerod. 85 (2000).
[16] J. Chen, L. Bao, Energy dissipation design with viscous dampers in high rise buildings, in: *Proceedings Of the 12th World Conference on Earthquake Engineering*, 2012.
[17] R. Mcnamara, D.P. Taylor, Fluid Viscous Damper for High Rise Buildings, Struct. Des. Tall Spec. Build. (2003).
[18] N. Makris, G.F. Dargush, M.C. Constantinou, Dynamic analysis of generalized viscoelastic fluids, J. Eng. Mech. 119 (1993).
[19] T. Asai, C.M. Chang, B.M. Phillips, B.F. Spencer, Real time hybrid simulation of a smart outrigger damping system for high-rise buildings, Eng. Struct. 57 (2013).
[20] G.W. Ho, The evolution of outrigger system in tall buildings, Int. j. high-rise build. 5 (2016).
[21] M. Malekinejad, R. Rahgozar, Free vibration analysis of tall buildings with outrigger-belt truss system, Earthq. struct. 2 (2011).
[22] P.R.K. Nanduri, B. Suresh, M.I. Hussain, Optimum position of outrigger system for high-rise reinforced concrete buildings under wind and earthquake loadings, Am. j. eng. res. 8 (2013).
[23] P.S. Kian, The use of outrigger and belt-truss system for high-rise concrete buildings, Civ. eng. dimens. 3 (2001).
[24] R. Rahgozar, Y. Sharifi, An approximate analysis of combined system of framed tube, shear core and belt truss in high-rise buildings, Struct. Des. Tall Special Build. 18 (2009).
[25] L. Cao, A. Downey, S. Laflamme, D. Taylor, J. Ricles, Variable friction device for structural control based on duo-servo vehicle brake: modeling and experimental validation, J. Sound Vib. 348 (2015) 41–56.
[26] L. Cao, S. Laflamme, D. Taylor, J. Ricles, Simulations of a variable friction device for multihazard mitigation, J. Struct. Eng. 142 (12) (2016) H4016001.
[27] J.N. Yang, J.H. Kim, A.K. Agrawal, Resetting semiactive stiffness damper for seismic response control, J. Struct. Eng. 126 (12) (2000) 1427–1433.
[28] J.A. Amin, A.K. Ahuja, Aerodynamic Modifications to the Shape of the Buildings: A Review of the State of the Art, 2010.

[29] M.F. Huang, Q. Li, C.M. Chan, W.J. Lou, K.C.S. Kwok, G. Li, Performance-based design optimization of tall concrete framed structures subject to wind excitations, J. Wind Eng. Ind. Aerod. 139 (2015) 70–81.
[30] S.H.I.K.I. Okamoto, N. Uemura, Effect of rounding side-corners on aerodynamic forces and turbulent wake of a cube placed on a ground plane, Exp. Fluid 11 (1) (1991) 58–64.
[31] Y.C. Kim, J. Kanda, Wind pressures on tapered and set-back tall buildings, J. Fluid Struct. 39 (2013) 306–321.
[32] Y.C. Kim, J. Kanda, Y. Tamura, Wind-induced coupled motion of tall buildings with varying square plan with height, J. Wind Eng. Ind. Aerod. 99 (5) (2011) 638–650.
[33] C.M. Chan, M.F. Huang, K.C. Kwok, Integrated wind load analysis and stiffness optimization of tall buildings with 3D modes, Eng. Struct. 32 (5) (2010) 1252–1261.
[34] H.E. Ilgın, M.H. Günel, The role of aerodynamic modifications in the form of tall buildings against wind excitation, ODTU Mimarlik Fakultesi Dergisi 24 (2) (2007) 17–25.
[35] J.P. Bitog, I.B. Lee, H.S. Hwang, M.H. Shin, S.W. Hong, I.H. Seo, Z. Pang, A wind tunnel study on aerodynamic porosity and windbreak drag, For. Sci. Technol. 7 (1) (2011) 8–16.
[36] K.P. You, Y.M. Kim, The wind-induced response characteristics of atypical tall buildings, Struct. Des. Tall Special Build. 18 (2) (2009) 217–233.
[37] F.M. Da Silva, M.G. Gomes, Gap inner pressures in multi-storey double skin facades, Energy Build. 40 (2008).
[38] K.S. Moon, Tall building motion control using double skin facades, J. Architect. Eng. 15 (2009).
[39] A. Azad, B. Samali, T. Ngo, C. Nguyen, Dynamic behaviour of flexible facade systems in tall buildings subjected to wind loads, Mater. Struct.: Advancement through Innovation (2013) 431–435.
[40] B. Samali, A. Azad, T. Ngo, Control of wind-induced motion of mid-rise buildings using smart facade systems, in: In Proceedings of the 6th Edition of the World Conference of the International Association for Structural Control and Monitoring (IACSM), Barcelona, Spain, 2014, pp. 2856–2863.
[41] G. Hu, S. Hassanli, K.C.S. Kwok, K.T. Tse, Wind-induced responses of a tall building with a double skin façade system, J. Wind Eng. Ind. Aerod. 168 (2017).
[42] G. Hu, J. Song, S. Hassanli, R. Ong, K.C.S. Kwok, The effects of a double skin façade on the cladding pressure around a tall building, J. Wind Eng. Ind. Aerod. 191 (2017).
[43] A. Giachetti, Wind Effects on Permeable Building Envelopes: A Two Dimensional Exploratory Study, Dissertation University of Florence, 2017.
[44] A. Giachetti, G. Bartolli, C. Mannini, Two-dimensional study of a rectangular cylinder with a forebody airtight screen at a small distance, J. Wind Eng. Ind. Aerod. 189 (2019) 11–21.
[45] G. Pomaranzi, N. Daniotti, P. Schito, L. Rosa, A. Zasso, Experimental assessment of the effects of a porous double skin façade system on cladding loads, J. Wind Eng. Ind. Aerod. 196 (2020).
[46] F. Hou, P.P. Sarkar, A. Alipour, A novel-mechanism-smart morphing façade system-to mitigate wind-induced vibration of tall buildings, Eng. Struct. 275 (2023).
[47] H.J. Gerhardt, F. Janser, Wind loads on wind permeable facades, J. Wind Eng. Ind. Aerod. 53 (1994).
[48] E. Maruta, M. Kanda, J. Sato, Effects on surface roughness for wind pressure on glass cladding of buildings, J. Wind Eng. Ind. Aerod. 74 (1998).
[49] W. Lou, M. Huang, M. Zhang, N. Lin, Experimental and zonal modeling for wind pressures on double skin facades of a tall building, Energy Build. 54 (2012) 179–191.
[50] H. Montazeri, B. Blocken, W.D. Janssen, V. Hoo, CFD Evaluation of New Second Skin Façade Concept for Wind Comfort on Building Balconies: Case Study for the Park Tower in Antwerp" *Building And Environment*, vol. 68, 2013.
[51] M. Jafari, A. Alipour, Aerodynamic shape optimization of rectangular and elliptical double-skin facades to mitigate wind-induced effects on tall buildings, J. Wind Eng. Ind. Aerod. 213 (2021).
[52] M. Jafari, A. Alipour, Review of Approaches, Opportunities, and Future Directions for Improving Aerodynamics of Tall Buildings with Smart Facades, Sustainable cities and society, 2021.
[53] American Institute of Steel Construction, ANSI/AISC 360-16 Specification for structural steel buildings, AISC (2016) 2005–2010.
[54] Asce (American Society of Civil Engineers), ASCE 07-16 Minimum Design Loads on Buildings and Other Structures, 2016.
[55] S. Preetha Hareendran, A. Alipour, B. Shafei, P.P. Sarkar, Performance-based wind design of tall buildings considering the nonlinearity in building response, J. Struct. Eng. 148 (2022).
[56] S.P. Hareendran, A. Alipour, B. Shafei, P. Sarkar, Characterizing wind-structure interaction for performance-based wind design of tall buildings, Eng. Struct. 289 (2023), 115812.
[57] S.P. Hareendran, A. Alipour, Prediction of nonlinear structural response under wind loads using deep learning techniques, Appl. Soft Comput. 129 (2022), 109424.
[58] W.H. Melbourne, T.R. Palmer, Accelerations and comfort criteria for buildings undergoing complex motions, J. Wind Eng. Ind. Aerod. 41 (1–3) (1992) 105–116.
[59] L. Micheli, L. Cao, S. Laflamme, A. Alipour, Life cycle cost evaluation strategy for high performance control systems under uncertainties, ASCE J. Eng. Mech. 146 (2) (2020) 1–15, 04019134.
[60] L. Micheli, A. Alipour, S. Laflamme, Life-cycle cost optimization of wind-excited tall buildings using surrogate models, J. Struct. Des. Tall Special Build. 30 (2021) 1–16. E1840.
[61] L. Micheli, A. Alipour, S. Laflamme, Multiple-surrogate models for probabilistic performance assessment of wind-excited tall buildings under uncertainties, ASCE-ASME J. Risk Uncertain. Eng. Syst. Part A Civ. Eng. 6 (4) (2020) 1–12, 04020042.
[62] L. Micheli, J. Hong, S. Laflamme, A. Alipour, Surrogate models for high performance control systems in wind-excited tall buildings, J. Appl. Soft Comput. 90 (2020) 1–15, 106133.
[63] D. Saini, A. Alipour, N.A. Heckert, E. Simiu, Design of high-rise buildings with arbitrary shapes for multi-directional wind, Structures 56 (2023), 105007.